Characterization of Nonlinear Material Damage Behavior Using Vibration Response Functions

Undergraduate Honors Thesis

By

Andrew M. Bialek

A Thesis Presented in Partial Fulfillment of the Requirements for

Graduation with Honors Distinction in the department of

Mechanical Engineering at The Ohio State University

Advisor:

Daniel A. Mendelsohn, Ph.D.

DEPARTMENT OF MECHANICAL AND AEROSPACE ENGINEERING

THE OHIO STATE UNIVERSITY

April 2013

ABSTRACT

The presence of cracks and other forms of material damage in structures can alter mode shapes and cause reductions in natural frequencies depending on their orientation. Previous research has examined high density microscopic dislocation behavior in the cohesive region of a crack. This behavior has been characterized by quadratic nonlinearities and hysteresis on a microscopic level. Current studies are limited to small amounts of this nonlinear behavior. This thesis presents a time domain analysis of the nonlinear longitudinal forced vibration of an elastic bar using the Finite Element Method. This study extends the types of solutions in previous research to include stronger nonlinearities previously limited by frequency domain methods. This formulation can also be later extended to include more general and complex nonlinear mechanisms than possible when using frequency domain approaches.

I would like to dedicate this paper to Samantha, whose patience is unequaled.

ACKNOWLEDGMENTS

First I would like to thank The Ohio State University for providing a scholarship to enhance my research experience. I would also like to thank Dr. Srinivasan for his insight. Finally, I would like to thank Dr. Mendelsohn. Without his persistence and expertise this project would not have been possible.

CONTENTS

LIST OF FIGURES

LIST OF TABLES

Chapter 1: INTRODUCTION

Vibration testing has historically been used to reduce noise and vibration in materials by characterizing modal frequencies and mode shapes of various structures. It has been well documented that the presence of cracks and other forms of material damage in structures can alter mode shapes and cause reductions in natural frequencies depending on their orientation. In Ref. [6], Natarajan et al. found significant reductions in natural frequencies of cracked functionally graded material plates by application of the Finite Element Method. It was observed that as crack length increases in a simply supported plate (Fig. (1a)), the fundamental frequency decreases due to a localized decrease in stiffness. Crack orientation also plays a significant role in the decrease of the fundamental frequency. The following Table 1 shows the effect of the crack orientation and crack length relative to plate size. It can be noted that the maximum reduction in fundamental frequency occurs for a crack oriented at 45 degrees relative to the base of the plate.

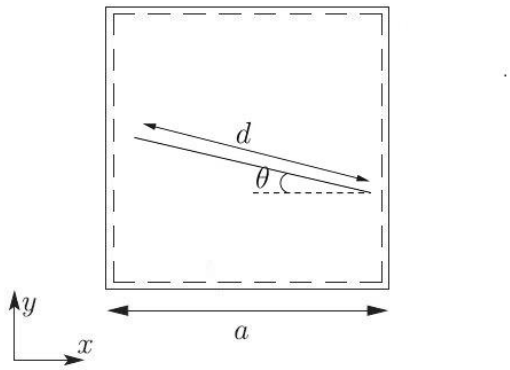

Figure 1: Simply Supported plate with center through crack (Courtesy Ref. [6])

Table 1: Non-Dimensionalized Fundamental frequency (Courtesy Ref. [6])

Crack orientation, θ	Crack length, d/a			
	0	0.4	0.6	0.8
0	3.0016	2.7383	2.5769	2.4747
10	3.0016	2.7356	2.5692	2.4583
20	3.0016	2.7315	2.5504	2.4130
30	3.0016	2.7259	2.5283	2.3594
40	3.0016	2.7220	2.5136	2.3223
45[a]	**3.0016**	**2.7202**	**2.5120**	**2.3170**
50	3.0016	2.7219	2.5135	2.3222
60	3.0016	2.7259	2.5283	2.3594
70	3.0016	2.7315	2.5504	2.4130
80	3.0016	2.7356	2.5692	2.4583
90	3.0016	2.7383	2.5770	2.4747

Figure (2) demonstrates the effect of crack location on fundamental frequency. The crack orientation was kept at $\theta = 0$ and the crack length held fixed and the position was varied. It was found that the minimum fundamental frequency occurs for cracks located at the center and the maximum occurs when the crack is situated at the corner [6]. Thus, the largest shift in fundamental frequency from the uncracked plate occurs at the center of the plate, and is reduced as much as 23% in this situation.

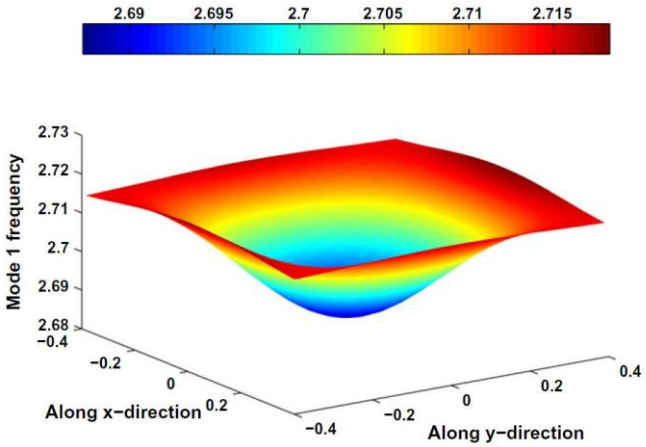

Figure 2: Fundamental Natural Frequency as a function of through crack position in a Simply Supported plate (Courtesy Ref. [6])

Knowledge of natural frequencies aids in the dynamic design of the structure; however, a key application of these types of analyses is in the inverse problem of

determining the location and size of cracks and the type and extent of other kinds of internal damage from the structure's vibration response or wave propagation and scattering signatures. In order to assist in the development of non-destructive testing systems to be used in practice there has been a considerable amount of research on the theoretical end to establish feasibility for a particular technique. These studies tend to establish orders of magnitude of the key effects and are only the beginning of the process of developing a device to be used in practice. The present research falls into the theoretical feasibility category. Much of the recent modeling of structural vibration testing related to crack detection and sizing has consisted of primarily linear elastic material behavior, see e.g. [6-10]. To the author's knowledge, only three types of nonlinear systems have been studied in this structural vibration context. The first nonlinear mechanism is known as the "breathing crack phenomenon", which studies the effect of repeated crack opening and closure. By coupling bending motion with longitudinal vibration, crack closure reduces by ½ the fundamental downward frequency shift due to the presence of the crack, see e.g. [11].

The second nonlinear mechanism studied considers nonlinear cohesive material behavior in the ligament ahead of the crack. Mendelsohn et al. [12-13] modeled an edge-crack in a beam with a cohesive zone ahead of the crack tip as a combination of a bending spring and a shear spring. A quasi-static fracture mechanics analysis of a cracked segment of beam with a nonlinear softening cohesive zone led to nonlinear force-displacement laws for the two springs. These force-displacement laws were used

for the springs in a free-vibration analysis of the damaged beam. The nonlinearity was dealt with by using a perturbation method valid for small amounts of nonlinearity in the frequency domain known as harmonic balancing. The result of this study shows the nonlinear free vibration spectra to contain the generation of a second harmonic. The higher harmonic that is generated is at least an order of magnitude smaller than the main response at the base frequency.

The third mechanism that is both nonlinear and dissipative is hysteresis. In Ref. [4] Mendelsohn and Pecorari study a simply supported beam that is modeled with a damage plane represented by nonlinear springs in the same context as in [12-13]. The linear portion of the spring law is used to account for first order discontinuities in displacement across the crack due to a lack of stiffness caused by a significant flaw or internal crack. The nonlinear spring with a quadratic hysteresis loop is used to account for some dissipative mechanism such as the repeated opening and closing of micro-cracks [14, 16, 17] in geomaterials and other quasi-brittle materials or high density dislocation motion [15] in the material in the highly stressed region ahead of the crack tip. This microscopic hysteretic behavior is characterized by the sliding of dislocations and defects in dislocation planes, and is a source of friction between these dislocation planes under fatigue or cyclic loading [15]. A damage parameter is then developed based on the product of the amplitude of free vibration with the ratio of nonlinear spring stiffness to that of the linear stiffness. This solution uses a slightly different perturbation harmonic balancing method than that in [12-13]. It is found that for any

given base natural vibration mode, the base natural frequency is shifted downward compared to the springs without the hysteretic terms, and further that the hysteresis leads to an infinite number of higher harmonics. Moreover due to the dissipation these effects all die out in time as the base frequency comes back to the linear value and the amplitudes of the harmonics go to zero. The aim of these studies has been more towards the feasibility of material damage characterization than merely flaw detection and sizing. The number of these types of studies has been increasing lately, particularly in a vibration setting. A number of other nontraditional vibration based methods that have been effectively applied in quantitatively characterizing various types of damage, fracture and creep failure in materials and structures have been surveyed in [5].

One of the primary tools in the experimental and modeling literature for nonlinear vibration characterization utilizes the forced vibration response due to harmonic excitation at a fixed driving frequency. Such a tool is used by Johnson and Guyer [14] to study the longitudinal motion of bars with and without nonlinearities. As is typical the forced response spectra was shown to be dependent on the amplitude and frequency of the harmonic forced excitation, typically represented as families of response spectra at various forcing amplitudes for the displacement, velocity or acceleration of some point on the bar. For a linear damped material, there are finite near resonant peaks that occur when the driving frequency exactly equals a free vibration natural frequency, as can be seen in Fig. (3) below in experimental results for Lucite.

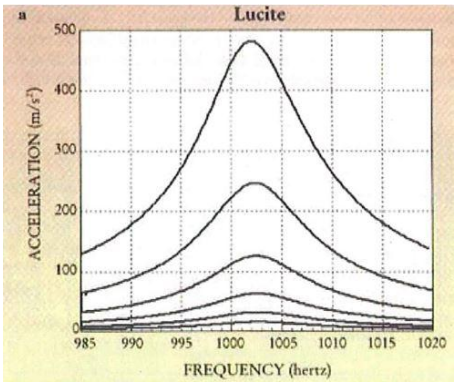

Figure 3: Response Spectra for Bar of Undamaged Lucite (Courtesy Ref. [14])

The introduction of nonlinearities, due to e.g. localized micro-cracking in quasi-brittle materials or dislocation motion in ductile metals, into the harmonically forced vibration problem has been shown to cause reductions in the peak frequencies of the response spectra. This decrease in peak frequency is dependent on the amplitude of the harmonic forcing. Johnson and Guyer used sandstone samples which exhibit hysteretic damage due to opening and closing of micro-cracks distributed throughout the bar and not localized at a macroscopic crack. The reduction in peak frequencies is seen clearly in Fig. (4) below, indicating the presence of the nonlinearity in the system. This type of nonlinear effect is the study of the present work.

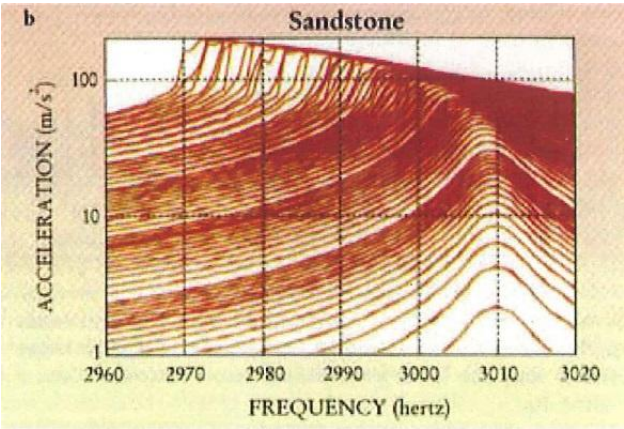

Figure 4: Response Spectra for Bar of homogenously damaged Sandstone (Courtesy Ref. [14])

This preliminary study of the dynamic nonlinear effects of spring type models for localized damage has extended the modeling capabilities in problems of this type of furthering the damage characterization of materials. To this end, a mathematical outline within which mechanisms such as nonlinear microstructural dislocation dynamic behavior can be accurately modeled has been developed in Ref. [4]. This framework can be used to characterize a second dynamic nonlinear effect known as hysteretic material damage behavior. This is accomplished using the nonlinear vibration response of laboratory type structures.

A similar study was conducted by Pecorari and Mendelsohn [18] in which a bar in forced longitudinal vibration of a bar with quadratic nonlinear hysteretic material behavior throughout the bar as opposed to the localized behavior in the free vibration study in Ref. [4]. The hysteresis is built into the stress-strain law in this model. A

perturbation analysis similar to that in Ref. [4] was used to find a linear relationship between the resonant frequency shift and the nonlinear attenuation of the excitation amplitude. One limiting facet of research done by Mendelsohn et al. [4, 12-13, 18] is that the solution methods follow a frequency domain approach and the asymptotic methods are valid only for small values of the damage parameters that control the strength of the nonlinearity.

The present investigation extends the type of solutions available for vibration problems with spring models of damage in Refs. [4] and [18] to include stronger nonlinearities by integrating the equations directly in time. A numerical approach is made in the present analysis using the Finite Element Method to discretize the system in space using a special element embodying the aforementioned nonlinear spring model to treat the damaged region. The resulting equations are then numerically integrated in time. While this method is computationally more intensive than frequency domain approaches, it allows for larger amounts of nonlinearities to be analyzed. These nonlinearities are studied within the response spectra for the harmonic forced vibration problem. Chapter 2 presents the formulation of the finite element vibration problem in addition to the corresponding boundary conditions. Chapter 3 presents numerical results that illustrate the displacement histories and spatial distributions along with the dependence of displacements on amplitude and driving frequency as a function of the nonlinearity. Of particular interest is the variation of the amplitude of the steady state

forced response with the driving force amplitude and with the driving force frequency near resonance. These are often indicative of a particular type of nonlinearity.

The original intent of this project was to study the hysteretic nonlinearity with the new time-domain formulation, however due to time limitations the quadratically nonlinear spring without hysteresis was chosen for the preliminary study. No attempt has been made here to close the loop and connect the constants in the nonlinear spring laws with a particular material mechanism or flaw geometry. Such work is the subject of future research.

Chapter 2: PROBLEM FORMULATION AND SOLUTION METHOD

1. Overview

The primary objective of the present work is to extend the modeling capabilities of the framework in [4] and [18] for treating localized nonlinear models for material damage in vibration problems. Currently the analysis for determining the free vibration natural frequencies and mode shapes and response to harmonic forcing of beams and bars is limited to asymptotically small amounts of nonlinearity. The current treatment is based on closed-form spatial solutions for the entire structure, and a harmonic expansion (Fourier series in time) and balance method to treat the dynamics. As such, this treatment is a frequency domain approach. This research implements a finite element approach for the spatial modeling and numerical time integration schemes to solve the resulting coupled system of ordinary differential equations (ODEs) and the localized nonlinear damage relations for nodal values of deflection and force adjacent on either side of the localized damage region. Several possible ways to model the localized damage in the FEM framework have been explored. The primary advantage of this time domain approach is that it is not limited to small amounts of nonlinearity. It will also be useful to compare to the perturbation approach for the same problem.

2. Problem Statement

The Finite Element Method is a numerical solution method for finding approximate solutions to partial differential equations (PDE's) and integral equations

[1]. In a steady state solution method, the differential equations are eliminated entirely resulting in large linear systems that are solved using linear algebraic techniques. The solution method explored in this analysis renders the PDE in space and time into a system of ODEs in time which are integrated using a variant of the Runge-Kutta method. The applications for FEM are vast, including but not limited to structural and vibration analysis of automotive, aerospace, biomechanical, and mechanical design disciplines. The present investigation consists of the structural analysis of a bar in forced longitudinal vibration, similar to that shown in Fig. (3) below. Both ends of the bar are forced with opposite magnitude and equal harmonic time dependence.

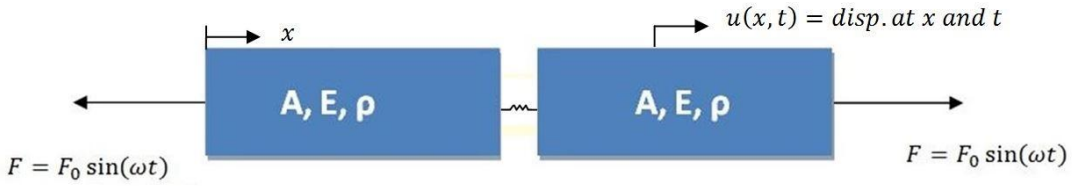

Figure 5: Axial Bar Loading with Spring Representing Localized Material Damage

The equation of motion for a bar in longitudinal motion with viscous damping and distributed loading is:

$$EA\frac{\partial^2 u}{\partial x^2} + f(x,t) + c\frac{\partial u}{\partial t} = \rho A\frac{\partial^2 u}{\partial t^2} \tag{1a}$$

where

$$u(x,t) = Displacement\ of\ Cross\ Section\ at\ x$$

$$f(x,t) = distributed\ loading\ (force\ per\ unit\ length\ in\ x)$$

$$b = Damping\ Constant$$

$$A = Cross\ Sectional\ Area$$

$$E = Young's\ Modulus$$

$$\rho = Density$$

The forcing at the ends of the bar can be represented by

$$f(x,t) = F_0 \sin \omega t\,[\delta(x-l) - \delta(x)] \qquad (1b)$$

where $\delta(x - x_0)$ is the Dirac delta function for an impulse or spike at $x = x_0$, [18].

$$\omega = \text{Driving Frequency}$$

$$F_0 = \text{Driving Amplitude}$$

The solution $\mathrm{u(x,t)}$ of Eq. (1a) is sought.

3. Shape Functions and the FEM Approximation

The system shown in Fig. (3) Is discretized into a finite number of elements, each with a given density, modulus of elasticity, and length. Within each element of our FEM discretization, the displacement at a point, x, in the element between the nodes of the ends is expressed in terms of polynomials. These polynomials are known as shape functions and allow for interpolation of the displacement between nodes [2]. In this analysis linear shape functions are assumed and use the global definition of x as position from the left end of the bar, Fig. 5.

$$N_L(x) = \frac{x_R - x}{l^e} \quad , \quad N_R(x) = \frac{x - x_L}{l^e} \qquad (2a)$$

Where $$l^e = x_R - x_L = \ Element\ length$$

$$x_L = Position\ of\ left\ node$$

$$x_R = Position\ of\ right\ node$$

$$x = Position\ of a\ point\ in\ element\ \ (x_L < x < x_R)$$

Figure 6: Left and Right Shape functions for a 1-D Element

The element shape function and nodal displacement vectors are defined as

$$\bar{N}^e = \left[N_L(x), N_R(x)\right]$$
$$\bar{a}^e = \begin{bmatrix} u_L(t) \\ u_R(t) \end{bmatrix} \qquad (2b)$$

and the FEM approximation for u(x,t) for an x in element e is then

$$u(x,t) = \bar{N}^e \cdot \bar{a}^e = \left[N_L(x), N_R(x)\right]\begin{bmatrix} u_L(t) \\ u_R(t) \end{bmatrix} = N_L(x)u_L(t) + N_R(x)u_R(t) \qquad (2c)$$

A global vector of shape functions $\bar{N}$ and nodal displacements $\bar{a}$ are constructed by combining the element shape function and nodal displacement vectors, respectively. The global shape function vector along with the nodal acceleration, velocity, and displacement vectors constitute the FEM approximation to $u(x,t), \dot{u}(x,t)$, and $\ddot{u}(x,t)$. Once the nodal displacement histories are solved for the solution for any quantity in the bar can be constructed. Note that the global shape function vector elements are defined such that if *x* is not in element *e*, then the shape

function for that element has a value of zero. These linear functions allow for continuity of displacement between elements, though, since they are constant throughout an element, stress and strain are discontinuous across element boundaries, as are the nodal forces.

4. Static Formulation

The principle of virtual work states that if a system in equilibrium under applied force is subjected to a virtual displacement, then the total virtual work of the system must be zero [3]. Thus, the work done by the external axial force through the virtual displacement must equal the work done by the internal stress through the internal virtual strain.

$$\int \delta u(x)\tilde{f}\,(x)dV = \int \delta\varepsilon(x)\sigma\,(x)dV \tag{3a}$$

The virtual displacement $\delta u(x)$ causes the strain $\delta\varepsilon(x)$ and $\tilde{f}(x)$ is the applied force per unit volume. The FEM approximations in terms of the global shape function vector $\bar{N}$ are

$$\bar{u} = \bar{N}\bar{a} \qquad \delta u = \bar{N}^T\delta\bar{a}$$

$$\delta\varepsilon = \bar{B}^T\delta\bar{a} \qquad \sigma = E\bar{B}\bar{a} \tag{3b}$$

Where $\bar{a}$ is the global vector of unknown nodal displacements and the vector $\bar{B}$ is the gradient of the global shape function vector and $\bar{B}^e$ is the element vector for $\bar{B}$, which is assembled from the $\bar{B}^e$ vectors in the same way as $\bar{N}$ is assembled from the $\bar{N}^e$ vectors

$$\bar{B} = \frac{d\bar{N}}{dx} \quad ; \quad \bar{B}^e = \left[-\frac{1}{l^e}, \frac{1}{l^e} \right] \tag{3c}$$

The usual definitions of normal stress and strain have been used.

$$\varepsilon = \frac{du}{dx} \text{ and } \sigma = E\varepsilon \tag{3d}$$

Using Eqs. (3b-d) Eq. (3a) can be rewritten as:

$$\delta\bar{a} \int \bar{N}^T \tilde{f}(x) dV = \delta\bar{a} \int \bar{B}^T E \bar{B} \bar{a}\, dV \tag{4}$$

For an arbitrary $\delta\bar{a}$, Eq. (4) reduces to:

$$\bar{K}\bar{a} + \bar{F} = \bar{0} \tag{5a}$$

Where the global stiffness matrix $\bar{K}$ is defined as

$$\bar{K} = \int \bar{B}^T E \bar{B}\, dV = \int_0^l EA \bar{B}^T \bar{B}\, dx = \sum_{e=1}^{l-1} \overline{K^e} \tag{5b}$$

and $\bar{K}^e$ is the element stiffness matrix

$$\bar{K}^e = \left(\frac{AE}{l} \right)_e \begin{bmatrix} 1 & -1 \\ -1 & 1 \end{bmatrix} \tag{5c}$$

The global applied force vector $\bar{F}$ is given by

$$\bar{F} = -\int \bar{N}^T \tilde{f}(x) dV = -\int_0^l \bar{N}^T f(x) dx = -\sum_{e=1}^{l-1} \int_{x_e}^{x_{e+1}} \int \bar{N}^T f(x) dx \tag{5d}$$

where *f(x)* is the applied force per unit length in x.

5. Dynamic Formulation

Eq. (5a) represents the governing equation of the static portion of the system presented in Eq. (1a). i.e.:

$$EA \frac{\partial^2 a}{\partial x^2} + f(x) = 0 \tag{6}$$

We treat the full dynamic equation in Eq. (1a) by using an alternate form of Newton's second law of motion hypothesized by 18th century French mathematician, Jean le Rond D'Alembert. The second law states simply that any force acting on a body is directly proportional to the mass times the acceleration of the body. D'Alembert postulated that in a dynamic setting applying a force that is the negative of the mass times the acceleration term is the same as including this inertia term in a positive sense on the right hand side of the second law as is usually done. D'Alembert's principle provides a convenient way to treat inertial terms [3], especially in computational settings such as these. Equation (1a) can then be rewritten as

$$EA\frac{\partial^2 u}{\partial x^2} + f_D(x,t) = 0 \tag{7a}$$

where f_D is a dynamic forcing function defined in a D'Alembert sense

$$f_D(x,t) = f(x,t) - c\frac{\partial u}{\partial t} - \rho A\frac{\partial^2 u}{\partial t^2} \tag{7b}$$

To obtain the dynamic FEM formulation from the static formulation, merely replace the static forcing vector $\overline{F}$ in Eq. (5d) with the following dynamic version:

$$\bar{F}_D(t) = -\int_0^l \overline{N}^T[f(x,t) - c\frac{\partial u}{\partial t} - \rho A\frac{\partial^2 u}{\partial t^2}]dx \tag{8a}$$

Using the FEM approximations in Eq. (3b) in Eq. (8a) we get:

$$\bar{F}_D(t) = \overline{F}(t) - \left(\int_0^l \rho A\overline{N}^T N\, dx\right)\ddot{\bar{a}}(t) - \left(\int_0^l c\overline{N}^T N\, dx\right)\dot{\bar{a}}(\mathrm{t}) \tag{8b}$$

where, using the forcing function in Eq. (1b), the applied forcing vector is given by

$$\overline{F}(t) = -\int_0^l \overline{N}^T f(x,t)dx = -\int_0^l \overline{N}^T F_0 \sin(\omega t)\,[\delta(x-l) - \delta(x)]dx \tag{8c}$$

Using the sifting property of the delta function [18], the forcing vector $\bar{F}(t)$ above is seen to have zero elements except for the 1st and Nth elements (at x = *0* and *l*) which are $-F_0 \sin(\omega t)$ and $+F_0 \sin(\omega t)$, respectively.

Plugging in this $\bar{F}_D(t)$ for $\bar{F}$ in Eq. (5a) then yields the dynamic governing FEM equations:

$$\overline{M}\ddot{\bar{a}}(t) + \overline{C}\dot{\bar{a}}(t) + \overline{K}\bar{a}(t) + \bar{F}(t) = 0 \tag{9}$$

where the global mass and damping matrices $\bar{M}$ and $\bar{C}$ are defined in the following, and the global stiffness matrix is given in Eq. (5b). Define first the matrix:

$$\begin{aligned}
\overline{\overline{M}} &= \int_0^l \bar{N}^T \bar{N} dx \\
&= \sum_{e=1}^{I-1} \int_{x_e}^{x_{e+1}} \bar{N}^{e^T} \bar{N}^e dx \\
&= \sum_{e=1}^{I-1} \int_{x_e}^{x_{e+1}} \begin{bmatrix} (N_e^e) \\ (N_{e+1}^e) \end{bmatrix} \begin{bmatrix} N_e^e & N_{e+1}^e \end{bmatrix} dx \\
&= \sum_{e=1}^{I-1} \int_{x_e}^{x_{e+1}} \begin{bmatrix} (N_e^e)^2 & (N_e^e)(N_{e+1}^e) \\ (N_e^e)(N_{e+1}^e) & (N_{e+1}^e)^2 \end{bmatrix} dx \\
&= \sum_{e=1}^{I-1} \int_{x_e}^{x_{e+1}} \begin{bmatrix} (N_e^e)^2 & (N_e^e)(N_{e+1}^e) \\ (N_e^e)(N_{e+1}^e) & (N_{e+1}^e)^2 \end{bmatrix} dx \\
&= \sum_{e=1}^{I-1} \begin{bmatrix} \widetilde{M}_{11}{}^e & \widetilde{M}_{12}{}^e \\ \widetilde{M}_{21}{}^e & \widetilde{M}_{22}{}^e \end{bmatrix} = \sum_{e=1}^{I-1} \overline{\overline{M}}^e = \sum_{e=1}^{I-1} \begin{bmatrix} \frac{1}{3} l_e & \frac{1}{6} l_e \\ \frac{1}{6} l_e & \frac{1}{3} l_e \end{bmatrix}
\end{aligned} \tag{10a}$$

Now define the global mass and damping matrices as

$$\overline{M} = \sum_{e=1}^{I-1} (\rho A)_e \overline{\overline{M}}^e \tag{10b}$$

$$\overline{C} = \sum_{e=1}^{I-1} (c)_e \overline{\overline{M}}^e \tag{10c}$$

This allows for the density, cross sectional area, and damping constant to vary element to element.

6. Damage Boundary Conditions and Damage Element

The simplest way to introduce the damage spring is through a damage finite element with length taken to be much shorter than the element length in the two intact portions of the bar. We are imagining applications in which a crack and damaged region is very thin and localized. Future work will include imposing boundary conditions directly on the two intact bar sections and assembling a new global system which includes auxiliary equations for the damage relations in addition to the normal FEM equations in the two intact bar sections. In that formulation the damaged region can be assigned an exactly zero width.

Due to the linear shape functions chosen nodal forces are discontinuous element to element in the intact bar portions, but it is assumed that there is no discontinuity in force across the very short damage element:

$$EA\left[\frac{\partial u}{\partial x}\right]_{-} = EA\left[\frac{\partial u}{\partial x}\right]_{+} \tag{7}$$

where the + and - refer to the leftmost node of the right portion of the bar and the rightmost node of the left portion of the bar, respectively. While the force is continuous across the damage element the displacement is not. The vibration solution will predict that the spring stretch (compression) will be sinusoidal between a negative

minimum and positive maximum. A negative stretch implies the two bar portions have interpenetrated each other, which is impossible. Therefore it is assumed that there is a quasi-static tensile preload on both ends of the bar. We do not add that load to the computation, which predicts only the dynamic motion superposed over the static displacements. If the damage does consist of a partial through crack and surrounding damage and the static preload were not used in the experimental setup then one would expect the two crack faces to be opening and then closing hard on each other, like clapping hands. The ensuing intermittent surface contact introduces additional nonlinear effects [8,11]. Mendelsohn et al. [13] discuss the necessity for a quasi-static preload to prevent the potential for mixing the two nonlinear effects. A second reason for using a quasi-static preload in an experimental setting is that it eliminates the need for very large vibration forcing amplitudes to induce nonlinear material behavior during vibration [13].

6a. Linear Damage Element

The damage element is shown schematically in Fig. 7. It is assumed first the standard linear spring force vs. stretch relation:

$$f_s = k_s \Delta S = k \tag{8}$$

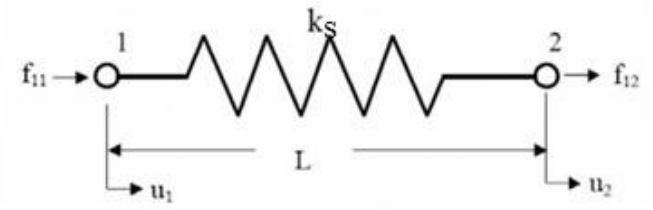

Figure 7: Damage Element

where $\Delta S = u_2 - u_1$ is the stretch in the spring from its neutral length L and f_s is the force in the spring. Noting from Eq. (7) that $f_s = f_{12} = -f_{11}$ we then have

$$f_{11} = k_s(u_1 - u_2) \tag{9a}$$

$$f_{12} = k_s(u_2 - u_1)$$

This can be written in matrix form as:

$$\begin{bmatrix} f_{11} \\ f_{12} \end{bmatrix} = \begin{bmatrix} k_s & -k_s \\ -k_s & k_s \end{bmatrix} \begin{bmatrix} u_1 \\ u_2 \end{bmatrix} \tag{9b}$$

Thus with $\bar{\boldsymbol{q}}^{\boldsymbol{i}} = \begin{bmatrix} \boldsymbol{f_{11}} \\ \boldsymbol{f_{12}} \end{bmatrix}$, $\bar{\boldsymbol{K}}^{\boldsymbol{i}} = \boldsymbol{k_s} \begin{bmatrix} \mathbf{1} & \mathbf{-1} \\ \mathbf{-1} & \mathbf{1} \end{bmatrix}$, and $\bar{\boldsymbol{a}}^{\boldsymbol{i}} = \begin{bmatrix} \boldsymbol{u_1} \\ \boldsymbol{u_2} \end{bmatrix}$ Eq. (9b) becomes:

$$\bar{\boldsymbol{q}}^{\boldsymbol{i}} = \bar{\boldsymbol{K}}^{\boldsymbol{i}} \bar{\boldsymbol{a}}^{\boldsymbol{i}} \tag{9c}$$

6b. Nonlinear Damage Element

As discussed in Chapter 1, the ability to approximate a crack with a nonlinear spring is consistent with the methodology used in Refs. [4] and [18] and is used in this analysis to model material degradation and damage. One such type of nonlinearity exhibits as local hardening or softening of the force-stretch relation, represented here by the quadratic term in the nonlinear spring element:

$$f_s = k_s \Delta S + k_Q (\Delta S)^2 \tag{10}$$

Where k_Q is the nonlinear stiffness parameter of the nonlinear damage element and represents hardening when positive and softening when negative. Results below are for hardening only. Future work will include softening and other more realistic forms of nonlinearity as well as dissipation in the form of hysteresis or viscous damping.

For demonstration, the stiffness matrix of a 6 node system with a nonlinear damage element at between nodes 3 and 4 is shown

$$\bar{K}=\begin{bmatrix} k_B & -k_B & 0 & 0 & 0 & 0 \\ -k_B & 2k_B & -k_B & 0 & 0 & 0 \\ 0 & -k_B & \{k_B+k_s+k_Q(u_4-u_3)\} & -\{k_s+k_Q(u_4-u_3)\} & 0 & 0 \\ 0 & 0 & -\{k_s+k_Q(u_4-u_3)\} & \{k_B+k_s+k_Q(u_4-u_3)\} & -k_B & 0 \\ 0 & 0 & 0 & -k_B & 2k_B & -k_B \\ 0 & 0 & 0 & 0 & -k_B & k_B \end{bmatrix} \tag{11}$$

The corresponding mass matrix is:

$$\underline{M}=\begin{bmatrix} 2\bar{\rho} & \bar{\rho} & 0 & 0 & 0 & 0 \\ \bar{\rho} & 4\bar{\rho} & 2\bar{\rho} & 0 & 0 & 0 \\ 0 & \bar{\rho} & 2\bar{\rho} & 0 & 0 & 0 \\ 0 & 0 & 2\bar{\rho} & 2\bar{\rho} & \bar{\rho} & 0 \\ 0 & 0 & 0 & \bar{\rho} & 4\bar{\rho} & \bar{\rho} \\ 0 & 0 & 0 & 0 & \bar{\rho} & 2\bar{\rho} \end{bmatrix} \tag{12}$$

Where $\bar{\rho}=\frac{1}{6}\rho Al$ and $(\rho A)_{e=3}$= 0 because it is assumed that the damage element is massless. Similarly, the corresponding damping matrix is:

$$\underline{C}=\begin{bmatrix} 2\bar{c} & \bar{c} & 0 & 0 & 0 & 0 \\ \bar{c} & 4\bar{c} & 2\bar{c} & 0 & 0 & 0 \\ 0 & \bar{c} & 2\bar{c} & 0 & 0 & 0 \\ 0 & 0 & 2\bar{c} & 2\bar{c} & \bar{c} & 0 \\ 0 & 0 & 0 & \bar{c} & 4\bar{c} & \bar{\rho} \\ 0 & 0 & 0 & 0 & \bar{c} & 2\bar{c} \end{bmatrix} \tag{13}$$

With $\bar{c}=\frac{1}{6}cl$ and assuming do damping in the damage element either, $(c)_{e=3}$ = 0.

The loading vector, as defined above for the end harmonic loads, is for this 6 node example

$$\bar{F} = \begin{bmatrix} -F_0 \sin \Omega t \\ 0 \\ 0 \\ 0 \\ 0 \\ F_0 \sin \Omega t \end{bmatrix} \tag{14}$$

7. Solution in the Time Domain

With all of the matrices and the force vector now properly defined for an N node, (N-1) element system Eq. (5) represents N coupled second order non-linear ODEs in the nodal displacements. These equations must be converted to a system of coupled first order ODEs in the nodal displacements and velocities. Consider the first equation of the system:

$$2\bar{\rho}\ddot{u}_1 + \bar{\rho}\ddot{u}_2 + 2\bar{c}\dot{u}_1 + \bar{c}_2\dot{u}_2 + k_B u_1 - k_B u_2 = -F_0 \sin(\Omega t) \tag{15}$$

This can be written as the following system of first order ODEs in u_1, u_2, v_1 and v_2 where v_1 and v_2 are the velocities of the first and second node, respectively.

$$U_1 = u_1 \tag{16}$$

$$U_2 = v_1$$

$$U_3 = u_2$$

$$U_4 = v_2$$

Where *U* is a vector of displacements and velocities:

$$U = \begin{bmatrix} U_1 \\ U_2 \\ U_3 \\ U_4 \end{bmatrix} = \begin{bmatrix} u_1 \\ v_1 \\ u_2 \\ v_2 \end{bmatrix}$$

Then its time derivative can be written as:

$$dU = \begin{bmatrix} v_1 \\ a_1 \\ v_2 \\ a_2 \end{bmatrix}$$

where $a_1 = \frac{dv_1}{dt}$ and $a_2 = \frac{dv_2}{dt}$. a_1 can be found by solving Eq. 15 above for $\ddot{u_1}$ and a_2 can be found by solving the second equation of the system for $\ddot{u_2}$ in a similar manner. If the same thing is done to all N of the second order equations in Eq. (5), then it is easily seen that 2N first order equations are obtained in the N unknown nodal displacements and N unknown nodal velocities. In the case of the nonlinear spring two of the equations will be nonlinear. If the nonlinear damage element is located between nodes s and s+1, referring to the 6 node illustrations above with the damage spring between nodes 3 and 4, we see that in the general case that the second of the two nonlinear equations [equation s+1 in Eq. (5)] takes the first order form

$$\begin{aligned} &2\bar{\rho}\frac{dv_s}{dt} + 2\bar{\rho}\frac{dv_{s+1}}{dt} + \bar{\rho}\frac{dv_{s+2}}{dt} + 2\bar{c}v_s + 2\bar{c}v_{s+1} + \bar{c}v_{s+2} \\ &\quad - k_s u_s - 2k_Q u_{s+1}u_s + k_Q u_s^2 + k_B u_{s+1} + k_s u_{s+1} + k_Q u_{s+1}^2 - k_B u_{s+2} = 0 \end{aligned} \tag{17}$$

The s equation has similar form.

The 2N first order ODEs are then integrated in time using ODE45. This routine uses a variant of the Runge-Kutta method to solve differential equations numerically [19]. It is a non-stiff solver of relatively high accuracy which uses automatic variable step sizing. The nonlinear terms are also handled automatically with no user input or direction. The default automatic step-size version of ODE45 was used throughout.

Although we are primarily interested in the forced response at the driving frequency ω, the solver requires specification of initial conditions. Zero initial displacement and velocity were used at each node. The following section contains preliminary results.

Not only will the FEM solution contain the solution due to the initial conditions, but it will also contain any possible rigid body motions. Since the configuration being considered in Fig. 5 is not fixed anywhere, rigid body motions will in fact be possible. The solution due to initial conditions is assembled from all the possible modes of free vibration of the system for both linear and nonlinear damage spring models. The rigid body motions of the (mass-spring-mass) system for a linear damage spring are easily found and the two natural frequencies for that motion are different still from the free vibration natural frequencies in the solution due to the initial conditions. All of these parts of the solution are present in the computed FEM time histories along with the primary desired part of the solution at the driving frequency due to the applied forces at the ends. In order to extract only this latter portion of the solution we take the Fast Fourier Transform of the FEM time histories and isolate the response amplitude at the driving frequency only.

Chapter 3: PRELIMINARY RESULTS

1. Mesh Convergence

In a finite element setting, determining the number of elements to use is crucial for accurate results. While using an infinite number of elements is ideal, minimization of computation time is also valuable. The response spectra obtained from the displacement histories (discussed in the next section) using the Fast Fourier Transform routine in Matlab were analyzed to find the peak frequency and amplitude in the neighborhood of a known natural frequency of the linear problem (solution not shown here). Convergence of the FEM discretization was tested by varying the number of nodes used. As the number of nodes was increased, the peak frequency of the response spectrum converged to about 5000 Hz, which corresponds to the second undamped linear natural frequency of the system. Fig. (8) below shows that this peak frequency convergence occurred around 240 nodes.

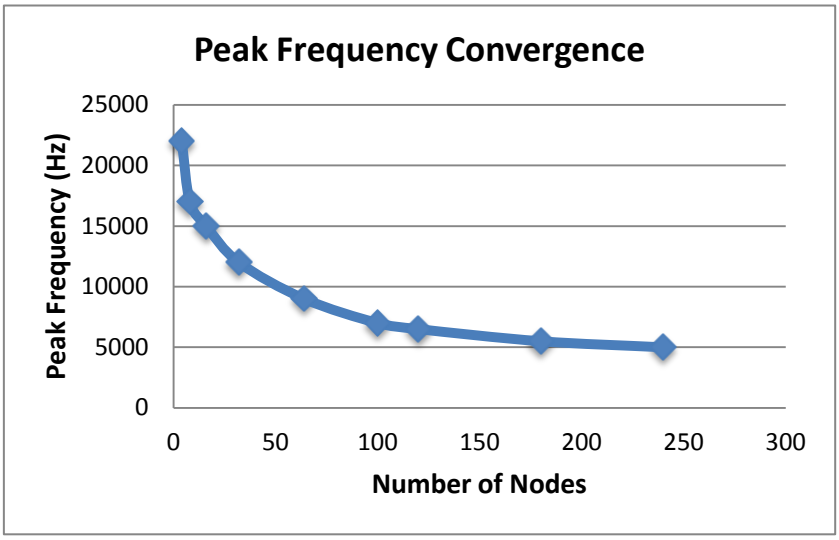

Figure 8: Finite Element Mesh Convergence

2. Displacement Spatial Distributions and Time Histories

The ratio of k_Q to k_S in equation 8b controls the strength of the nonlinearity and was the studied effect. This ratio was studied from values of k_Q=0 (linear system) to k_Q=5.5 k_S, which was the maximum value for which the MATLAB ODE45 solver was able to compute a solution. For values of k_Q larger than 5.5 k_S the solution diverged and made no sense. The values of all the other material constants and bar geometry are E = $200E9\ \frac{N}{m^2}$, ρ = $7800\ \frac{kg}{m^3}$, c = $10^6\ \frac{N*s}{m}$, A = 0.1 m^2, L = 1 m. Figure 9 shows the effect of an increasing value of the nonlinearity on the slope of the displacement jump between adjacent nodes in the damaged region. This jump in displacement is characteristic of the ΔS term in Eq. (8b) and can be seen in Fig. (9a,b). for a spring of width 1/1000 of the constant element length in the intact bar. The plots are versus node number and the damage spring is between nodes 50 and 51. As can be seen in Fig. 9 this very short element length between nodes 50 and 51 is not illustrated on these plots, rather the element appears to be the same length as in the bar. Imagine instead that node 51 data points lie almost directly below their corresponding node 50 data point. Figure 9b shows a close-up of this region in which the horizontal scale is greatly exaggerated.

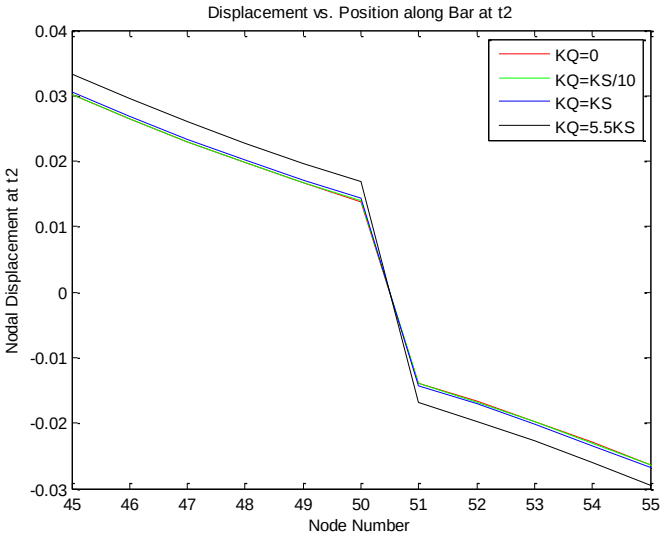

Figure 9a: Displacement Jump with Increasing Nonlinearity

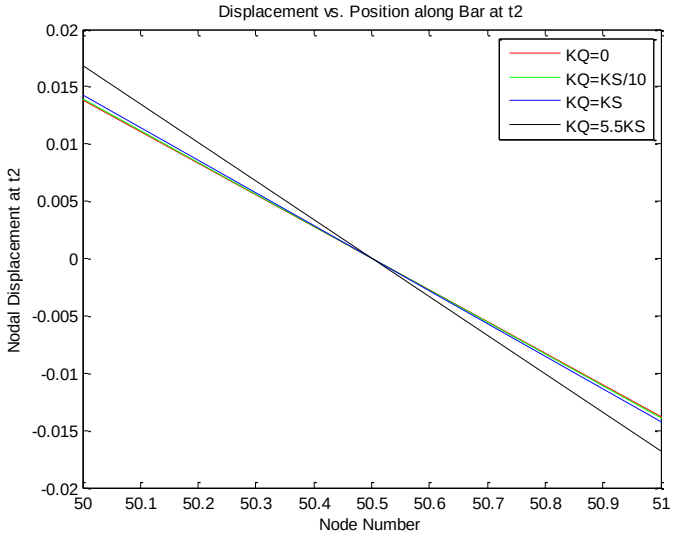

Figure 9b: Close-up of Displacement Jump with Increasing Nonlinearity

As the strength of the nonlinearity increases, the slope of this displacement jump also increases. This result is puzzling since a positive K_Q represents a quadratic hardening spring. This should lead to higher spring forces and smaller displacement jumps as K_Q increases relative to K_S and the overall stiffness of the spring increases as well. If the spring were softening the stiffness goes down as the absolute value of k_Q increases and we would expect the kind of behavior found here. This will be topic of further investigation.

Figure 10 shows a typical time history of the displacement of the right end of right bar section (x = l). The period corresponding to the forced response at the driving frequency is shown on the figure. The presence of other frequencies in the response is obvious.

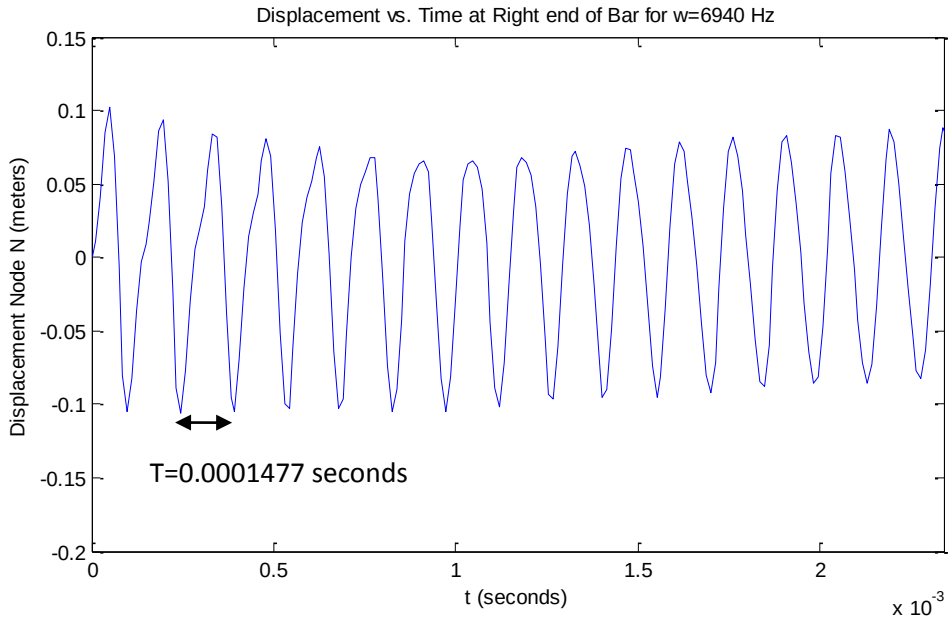

Figure 10: Time History for Driving Frequency of 6,940 Hz.

3. Dependence of Displacements on Amplitude and Driving Frequency

Due to the presence of rigid body motion and the transient solution due to the initial conditions along with the forced response at the driving frequency the displacement histories were subjected to a Fast Fourier Transform to obtain only the nodal amplitude at a location along the bar at the driving frequency. For a linear system ($k_Q = 0$) the effect of the increase of the harmonic forcing amplitude on the peak frequency in the response spectra was studied. Fig. (10) below shows these results for a range of forces between 1E11 to 7E11 N.

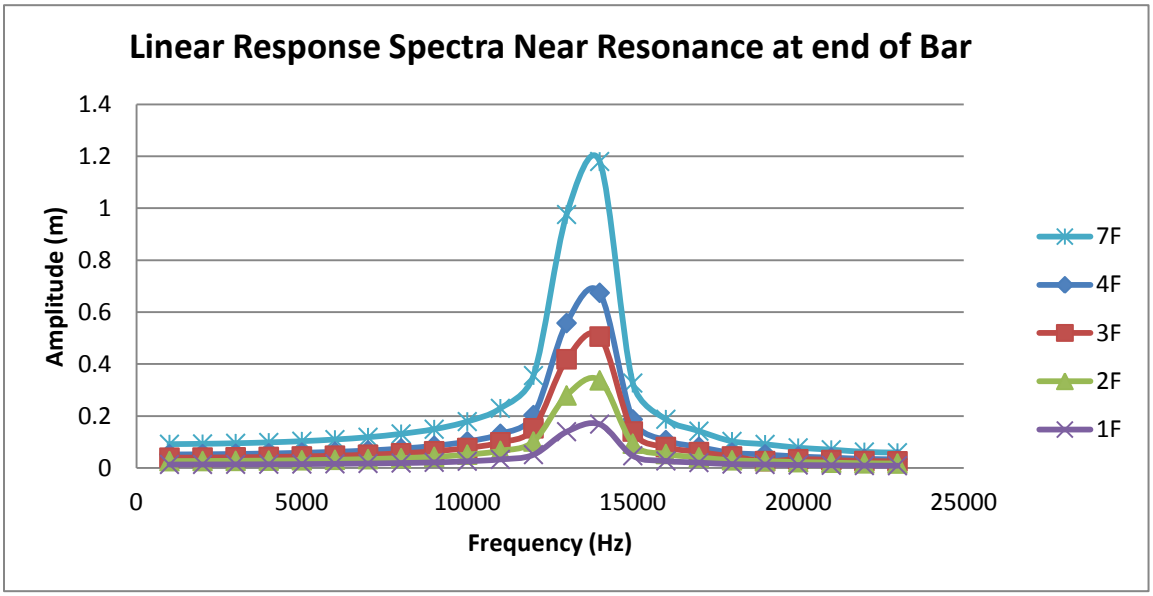

Figure 10: Effect of Harmonic Forcing Amplitude on Displacement Amplitude

The resonant or peak frequency and the shape of the spectrum near resonance are unchanged by the increase in the magnitude of the applied force, and the peak amplitude scales linearly with the applied force amplitude. This behavior is consistent

with that shown in Fig. (3) and is characteristic of a structure lacking nonlinear material behavior.

For a constant nonlinear ratio of $K_Q=0.5K_s$, a similar study of the effect of the increase of the harmonic forcing amplitude on the peak frequency in the response spectra was carried out. Fig. (11). below shows these results for a range of forces between 1E11 to 7E11 N.

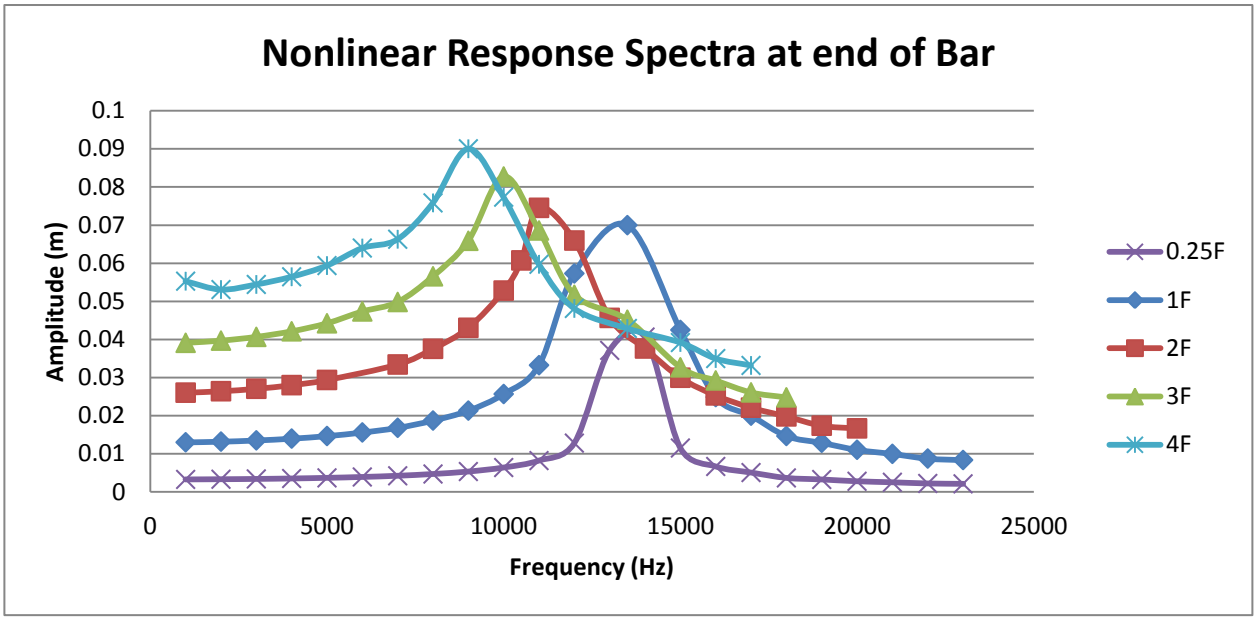

Figure 11: Effect of Harmonic Forcing Amplitude on Peak Frequency

As the harmonic forcing amplitude increases, there is a distinct decrease in the peak frequency, which can be more clearly seen in Fig. (13). This behavior is consistent with that shown in Fig. (4) and is characteristic of nonlinear material behavior.

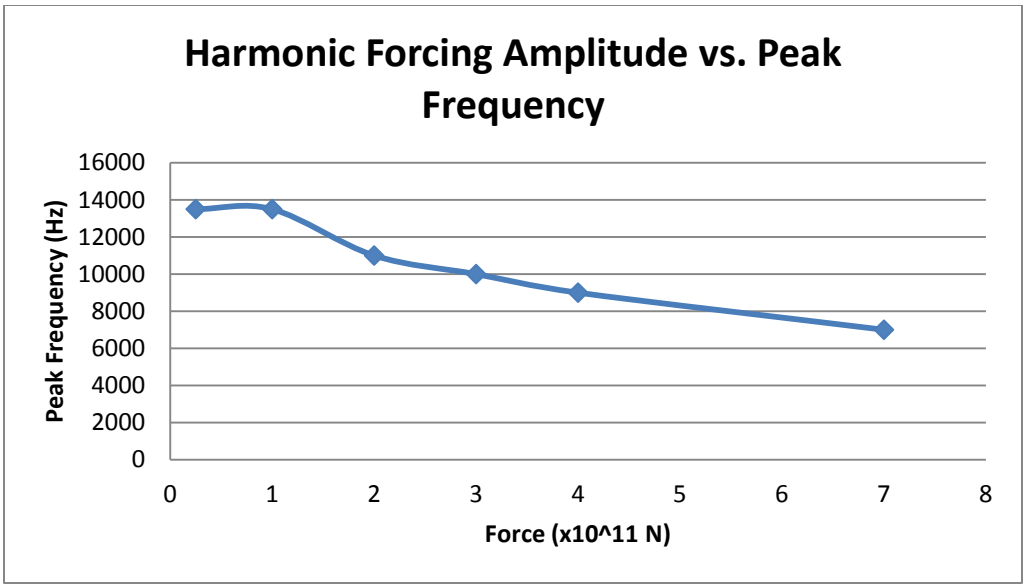

Figure 12: Decrease in Peak Frequency due to Nonlinear Behavior

There is a distinct and nearly linear decrease in the peak frequency as the harmonic forcing amplitude increases. It takes a force of a high enough magnitude to excite this nonlinear behavior, however, which computationally makes sense. Referring back to Eq. (8b), the influence of the quadratic stiffness term is influenced by the square of the value of the displacement jump in the damaged element, ΔS. If this term is insignificantly small, the nonlinear effect also becomes negligible. This explains why there is no visible decrease in the peak frequency between 0.25F and 1F. Further numerical experiments are needed to discern the effects at lower and more realistic values of the forcing amplitude than used here.

Chapter 4: CONCLUSION

1. Goals Met

The original intent of this project was to study the hysteretic nonlinearity with the new time-domain formulation. Time limitations required the study to be limited to a quadratically nonlinear spring without hysteresis. The objective of the study was to extend the modeling capabilities of the framework in [4] and [18] for treating localized and distributed nonlinear models for material damage in vibration problems. This modeling capability has been extended from a perturbation based Frequency Domain approach limited to small amounts of nonlinearity to the Time Domain approach presented herein, which is valid for larger amounts of nonlinearity.

2. Contributions

This research assists in the theoretical feasibility for development of non-destructive testing systems designed to locate and characterize damage in a structure. Recent modeling of structural vibration testing in crack detection and sizing has dealt with primarily linear elastic material behavior. Mendelsohn et al., however, have contributed to studies in the nonlinear domain of this type of structural vibration testing. The aim of these studies has been to study the feasibility of damage characterization as opposed to merely flaw detection and sizing. In a forced vibration problem Pecorari and Mendelsohn attempted to find a linear relationship between the resonant frequency shift and the nonlinear attenuation of the excitation amplitude. This research extends the type of solutions available for vibration problems with spring

models of damage in both free vibration [4] and forced vibration [18] settings to include stronger nonlinearities.

3. Summary of Preliminary Results

The strength of the nonlinearity was the studied effect in both spatial distributions and time histories. The ratio of k_Q to k_S was studied between values of 0 and 5.5. It was found that increasing the value of the nonlinearity increased the slope of the displacement jump, which is the opposite effect as expected. A positive k_Q represents a quadratic hardening spring, which should result in smaller displacement jumps. The behavior exhibits that characteristic of spring softening and will be investigated further.

The typical time histories of displacements calculated at a point along the bar exhibited the presence of other frequencies. This is characteristic of rigid body motion and the transient solution from initial conditions which are combined with the forced response at the driving frequency. As such, a Fast Fourier Transform was conducted to obtain nodal amplitudes at the driving frequency. For the linear system, the peak amplitude was found to scale linearly with the applied force amplitude, which is consistent with longstanding experimental results and theory for the linear problem. For a nonlinear system, as the harmonic forcing amplitude increases, there is a nearly linear decrease in the peak frequency. This too is characteristic of many previously modeled and measured nonlinear vibrating systems.

4. Recommendations for Future Work

In addition to continuing to investigate the nature of the nonlinear spring as it models material damage, a hysteretic nonlinearity which also models the damping typical of damaged material will be studied. A subject of future research may include an attempt to connect the constants in the nonlinear spring laws with specific flaw geometry and material mechanisms, though present work falls under the realm of theoretical feasibility studies using phenomenological models in which the parameters lack direct physical meaning at this time.

REFERENCES

1. Dupaix, Rebecca: ME 5139 Lecture Notes *"The Finite Element Method Introduction"*

2. Sanford, R.J, *Principles of Fracture Mechanics*. Pearson Education, 2003. p. 142.

3. Rao, Singiresu. Mechanical Vibrations (4th Edition). New Jersey: Prentice Hall, 2004: 110-111.`

4. Mendelsohn, Daniel A, and Claudio Pecorari. "Nonlinear Free Vibrations of a Beam with Hysteretic Damage." Journal of Sound and Vibration (2012): 1-14

5. Gibson, Ronald F. "Nontraditional Applications of Vibration Testing for Material Characterization." 2003 2003 SEM Annual Conference & Exposition on Experimental and Applied Mechanics (2002): 1-2. 26 Sep. 2012

6. S. Natarajan, P.M. Baiz, S. Bordas, T. Rabczuk, P.Kerfriden. "Natural Frequencies of Cracked Functionally Graded Material Plates by the Extended Finite Element Method." Journal of Composite Structures (2011): 3082-3092.

7. A. D. Dimarogonas, "Vibration of cracked structures: A state of the art review," Engng Frac. Mech. 55, 831-857 (1996).

8. T. G. Chondros, A. D. Dimarogonas, and J. Yao, "Vibration of a beam with a breathing crack," J. Sound Vib. 239, 57-67 (2001).

9. J. A. Brandon, E. M. O. Lopez, and A. E. Stephens, "Spectral indicators in structural damage identification: a case study," *J. Mech. Engng. Sci.-Proc.Inst. Mech. Engnrs. C* 213, 411-415 (1999)

10. A. S. Sekhar and P. Balaji Prasad, "Crack identification in a cantilever beam using coupled response measurements," *J. Engng. Gas Turb. Power* 120, 775-777 (1998).

11. R. Ruotolo, C. Surace, P. Crespo, and D. Storer, "Harmonic analysis of the vibrations of a cantilevered beam with a closing crack," Comp. Struct. 61, 1057-1074 (1996).

12. P. S. Mokashi and D. A. Mendelsohn, “Nonlinear vibration of an edge-cracked beam with a cohesive zone, I: Nonlinear bending load-displacement relations for a linear softening cohesive law,” J. Mech. Matls. Struct. 3, 1573-1588 (2008).

13. D. A. Mendelsohn, S. Vedachalam, C. Pecorari, and P. S. Mokashi, “Nonlinear vibration of an edge-cracked beam with a cohesive zone, II: Perturbation analysis of Euler-Bernoulli beam vibration using a nonlinear spring for damage characterization,” J. Mech. Matls. Struct. 3, 1589-1604 (2008).

14. R. A. Guyer and P. A. Johnson, "Nonlinear mesoscipic elasticity: Evidence for a new class of material",Physics Today, pgs. 30-36, April (1999).

15. A. Granato, K. Lücke, Theory of mechanical damping due to dislocations, *J. Appl. Phys*. 27, 583-593 (1956).

16. V. Gusev, “Theory of non-collinear interactions of acoustic waves in an isotropic material with hysteretic quadratic nonlinearity,” *J. Acoust. Soc. Am.* 111, 80-94 (2002).

17. V. Gusev, “Propagation of acoustic pulses in material with hysteretic nonlinearity,” *J. Acoust. Soc. Am.* 107, 3047-3058 (2000).

18. C. Pecorari and D. A. Mendelsohn, “Nonlinear Forced Vibrations of a Hysteretic Bar: Revisited”, *Wave Motion*, Vol. 50, Issue 2 March, 127-134 , 2013.

19. Srinivasan, Manoj, Lecture on Integrating ODEs for Dynamic Systems. February 2013.

MATLAB Input Code

```
%Finite Element Analysis of Free-Free Bar in Longitudinal Forced
Vibration
%Author: Andrew M Bialek
%Date: Feb 4th 2013

%----------------------------------PRE-PROCESSING----------------------
clc

%dbstop if error
N=240; %Number of Nodes
w=7000*2*pi ;
F=1E11; %Forcing Amplitude (N)
t1=0; %Lower Time Limit
t2=0.001;%((2*pi)/w)*14; %Upper Time Limit
Numtimelist = 200; % Number of Timepoints to solve at in between t1 and
t2.
Samplefreq=(Numtimelist/t2);
tspan = linspace(t1,t2,Numtimelist)'; %Time Vector
statevar0 = zeros(2*N,1); %Initial Conditions for State Variable [u1,
du1, u2, du2...etc]
options = odeset('reltol',1e-9,'abstol',1e-9); %ODE 45 Accuracy Options



%Parameters-------------------------------------------------------------
---------
S=N/2; %Damaged Region
S=round(S);
L=1/N; %Element Length (Bar Length=1)
LS=L/1000; %Length of Spring Element
E=200E9; %Modulus
rho=7800; %Density
%F=1E11
C = 10^6; %Damping coefficient
KB =(100*E); %Stiffness of 1-D Bar Elements Surrounding Damaged Region
KS =(2*10^12); %Linear Spring at Damaged Region
KQ = 0; %Nonlinear Stiffness
%100000
A=0.1;  %Cross Sectional Area (m^2)
%ODE Passed Parameters--------------------------------------------------
--------------
param.E = E;  %Modulus (N/m^2) Steel
param.rho = rho; %Density (kg/m^3)
param.A = A; %Cross Sectional Area (m^2)
param.L = L; %Element Length (m)
param.w =  w ; %Frequency (rad/sec)
param.F = F; %Forcing Amplitude (N)
param.N = N; %Number of Nodes
param.S= S; %Damaged Region Location
param.LS= LS;
```

```
param.Numtimelist = Numtimelist;

%----------------------------------PROCESSING-------------------------
-----------------
%----------------------------------------------------------------------
-----------------
%----------------------------------------------------------------------
-----------------

[tlist_100000_3F,statevarlist_100000_3F] =
ode45(@ODERHS_Omega_100000_3F,tspan,statevar0,options,param);
%LHS=FUNCTION OUTPUTS
%RHS=FUNCTION INPUTS

%----------------------------------POST-PROCESSING--------------------
-----------------
%----------------------------------------------------------------------
-----------------
%----------------------------------------------------------------------
-----------------

a=1;
ulist_100000_3F=zeros(Numtimelist,N);
dulist_100000_3F=zeros(Numtimelist,N);

for i=1:N

ulist_100000_3F(:,i) = statevarlist_100000_3F(:,a);
a=a+1;
dulist_100000_3F(:,i)= statevarlist_100000_3F(:,a);
a=a+1;

end

%DISPLACEMENT VS. TIME PLOT

Dispjump= (ulist_100000_3F(:,S+1)-ulist_100000_3F(:,S));
Nonlin=(((Dispjump.*KQ)./KS).*100);

figure(2)
plot(tlist_100000_3F,Dispjump);ylabel('Jump in Displacement from Node S
to S+1');xlabel('t')

figure(3)
plot(tlist_100000_3F,(ulist_100000_3F(:,N))); ylabel('Displacement Node
N (meters)');xlabel('t (seconds)')
title('Displacement vs. Time at Right end of Bar')


%DISPLACEMENT VS. NODE PLOT
```

```
xnode=1:1:N; %Node Vector for Displacement vs. Position Plot
disp=ulist(Numtimelist,1:N); %Displacement Vector for Displacement vs.
Position Plot
figure(4) %Displacement vs. Position Plot
plot(xnode,disp); ylabel('Nodal Displacement at t=0.012
seconds');xlabel('Node Number (x= 1 to N)')
title('Displacement vs. Position along Bar at T=0.012 seconds')

%%%%%%%%%%%%%%%%%%%%%%%%%%%%%%%%%%%%%%%%%%%%%%%%%%%%%%%%%%%%%%%%%%%%%%%%%%%%
%%%


%FAMILIES OF PLOTS%%%%%%%%%%%%%%%%%%%%%%%%%%%%%%%%%%%%%%%%%%%%%%%%%%%%%%%%%

%DISPLACEMENT VS. NODE PLOT

% xnode2=1:1:N; %Node Vector for Displacement vs. Position Plot
% disp0=ulist_KQ_0_With_Static_F_Adjusted(200,1:N);
% disp1=ulist_KQ_1_10KS_With_Static_F_Adjusted(200,1:N); %Displacement
Vector for Displacement vs. Position Plot
% disp2=ulist_KQ_KS_With_Static_F_Adjusted(200,1:N);
% disp3=ulist_KQ_10KS_With_Static_F_Adjusted(200,1:N);
% disp4=ulist(200,1:N);
% figure(7) %Displacement vs. Position Plot
% plot(xnode2,disp0,'r');
% hold on
% plot(xnode2,disp1,'g');
% plot(xnode2,disp2,'b');
% plot(xnode2,disp3,'k');
% plot(xnode2,disp4,'m');
% hold off
% ylabel('Nodal Displacement at t2');
% xlabel('Node Number');
% title('Displacement vs. Position along Bar at t2');
% legend('KQ=0','KQ=KS/10','KQ=KS','KQ=10KS','KQ=100KS');


%FFT PLOTS
%%%%%%%%%%%%%%%%%%%%%%%%%%%%%%%%%%%%%%%%%%%%%%%%%%%%%%%%%%%%%%%%%%%%%%%%%%%%

Fs = Samplefreq;              % Sampling frequency
T = 1/Fs;                     % Sample time
L = 1000;                     % Length of signal
t = (0:L-1)*T;                % Time vector
PeriodRed=Numtimelist*(1/1);

y=ulist_100000_3F(1:PeriodRed,N)        ;               %Original
Signal
Dispjump= (ulist_100000_3F(:,S+1)-ulist_100000_3F(:,S));
```

```
% NFFT = 2^nextpow2(L); % Next power of 2 from length of y
% Y = fft(y,NFFT)/L;
% f = Fs/2*linspace(0,1,NFFT/2+1);

% % Plot single-sided amplitude spectrum.
% figure(11)
% plot(f,2*abs(Y(1:NFFT/2+1)))
% title('Single-Sided Amplitude Spectrum of Node N @ KQ=0')
% xlabel('Frequency (Hz)')
% ylabel('|Y(f)|')


NFFT2 = 2^nextpow2(L); % Next power of 2 from length of y
Y2 = fft(Dispjump,NFFT2)/L;
f2 = Fs/2*linspace(0,1,NFFT2/2+1);

figure(5)
plot(f2,2*abs(Y2(1:NFFT2/2+1)))
title('Single-Sided Amplitude Spectrum of Displacement Jump @ KQ=0 ')
xlabel('Frequency (Hz)')
ylabel('|Y(f)|')
```

ODE 45 Code

```
function dU = ODERHS_Omega_100000_3F(t,U,param)



%------------------------UNPACKING AND ESTABLISHING PARAMETERS
E = param.E; rho = param.rho;
A = param.A; L = param.L;
w = param.w; F = param.F; N = param.N;
S = param.S; LS =param.LS;
%Numtimelist = param.Numtimelist;
C = 10^6; %Damping coefficient
KB =(100*E); %Stiffness of 1-D Bar Elements Surrounding Damaged Region
KS =(2*10^12); %Linear Spring at Damaged Region
KQ = KS/2; %Nonlinear Stiffness
%Start KS/10

%Shape Function Parameters
M11=rho*A*(L/3);
M12=rho*A*(L/6);
M21=rho*A*(L/6);
M22=rho*A*(L/3);
C11=(L/3);
C12=(L/6);
C21=(L/6);
C22=(L/3);
NODE= M22+M11;
NODES=C22+C11;
M11S=0;%rho*A*(LS/3);
M12S=0;%rho*A*(LS/6);
M21S=0;%rho*A*(LS/6);
M22S=0;%rho*A*(LS/3);
C11S=0;
C12S=0;
C21S=0;
C22S=0;


%------------------------------ASSEMBLE U AND DU MATRICES

y=1; %index
u=zeros(N,1);
du=zeros(N,1);

    for i=1:N

         u(i,1) = U(y,1);
         y=y+1;
         du(i,1) = U(y,1);
         y=y+1;
```

```
    end

MASS=zeros(N); %Initialize Mass Matrix, Force Matrix, Stiffness Matrix
R=zeros(N,1);
K0=zeros(N);
R(N,1) = F*sin(w*t);%+F/6*sin(2*t);
R(1,1) = -F*sin(w*t);%-F/6*sin(2*t);


%------------------------------ASSEMBLE M AND K MATRICES
MASS(1,1)=M11;
MASS(1,2)=M12;

DAMP(1,1)=C11;
DAMP(1,2)=C12;

K0(1,1)=KB;
K0(1,2)=-KB;

    for i=1:N-1

    MASS(i+1,i)=M21;

    MASS(i+1,i+1)=NODE;

    MASS(i+1,i+2)=M12;

    DAMP(i+1,i)=C21;

    DAMP(i+1,i+1)=NODES;

    DAMP(i+1,i+2)=C12;

    K0(i+1,i)=-KB;

    K0(i+1,i+1)=(2*KB);

    K0(i+1,i+2)=-KB;

    end

    MASS(N,N)= MASS(1,1);
   K0(N,N) =  abs(K0(N,N+1));
   DAMP(N,N)=DAMP(1,1);
%------------------------------INTRODUCE DAMAGED REGION

%    Damaged Region without Mass or Damping
    MASS(S,S) = (M11+M11S);
    MASS(S+1,S+1) = (M22S+M22);
```

```
    MASS(S,S+1) = (M12S);
    MASS(S+1,S) = (M11S);

    DAMP(S,S) = (C11+C11S);
    DAMP(S+1,S+1) = (C22S+C22);
    DAMP(S,S+1) = (C12S);
    DAMP(S+1,S) = (C11S);

% %   Linear Spring Stiffness at Damaged Region
%     K0(S,S) = KS+KB;
%     K0(S+1,S+1) = KS+KB;
%     K0(S,S+1) = -KS;
%     K0(S+1,S) = -KS;

%    Nonlinear Stiffness
    JUMP=(u(S+1)-u(S));
    NonLinStiff1= KS+KQ*JUMP; % u(S)-u(S-1)
    NonLinStiff2= -KS-KQ*JUMP;
    K0(S,S) = NonLinStiff1 + KB;
    K0(S+1,S+1) = NonLinStiff1 + KB;
    K0(S,S+1) = NonLinStiff2;
    K0(S+1,S) = NonLinStiff2;


TOOS=[   (((KQ*JUMP^2)/KS)*100), t, JUMP, KQ/KS, 28940/100000 ];

% %    %if KQ*JUMP/KS < 1
%    disp('% Nonlinearity| Time | JUMP  |  KQ/KS  | w')
%    disp(TOOS)
  % else
   %end

%-------------------------------BOUNDARY CONDITIONS----------------------
MASSRED=MASS(1:N,1:N);
CRED=DAMP(1:N,1:N);
KRED=K0(1:N,1:N);
FRED=R(1:N,1);
% u(1,1)=0;
% du(1,1)=0;

%-----------------------------------PROCESSING---------------------------

Q= (FRED - C*CRED*du - KRED*u);


DD=((MASSRED)\Q);

%Alternate Solving Method
%DD= ((((MASSRED))\((FRED-(KRED*u)))) - C*du);

j=1; %index
```

```
ddu=zeros(1,N);
    for i=1:N

    ddu(i) = DD(j);

    j=j+1;

    end

b=1; %index
% du(1)=0;
% ddu(1)=0;

dU=zeros(2*N,1);
    for i=1:N

    dU(b,1) = du(i);
    b=b+1;
    dU(b,1) = ddu(i);
    b=b+1;

    end


% xnode=1:1:N; %Node Vector for Displacement vs. Position Plot
% displacement=u(1:N,1); %Displacement Vector for Displacement vs.
Position Plot
% figure(4) %Displacement vs. Position Plot
% plot(xnode,displacement); ylabel('Nodal Displacement at t=T
seconds');xlabel('Node Number (x= 1 to N)')
%  title([ 'Displacement vs. Position along Bar at t=  ', num2str(t,3)]
);


end
```